

SEARCHES FOR GIANT PULSES FROM EXTRAGALACTIC PULSARS

M. A. McLAUGHLIN¹ & J. M. CORDES²
Draft version May 9, 2019

ABSTRACT

We discuss the giant-pulse phenomenon exhibited by pulsars and the distances to which giant pulses might be detected from extragalactic pulsars. We describe the conditions under which a single-pulse search is more sensitive than a standard periodicity search. We find that, for certain pulse-amplitude distribution power laws and time series lengths, single-pulse searches can be superior. We present the results of searches toward several extragalactic targets, including M33, the LMC (PSR B0540–69) and several other galaxies. While we have not conclusively detected giant pulses from any of these targets, these searches illustrate the methodology of, issues related to and difficulties in these types of searches.

Subject headings: pulsars, radio pulses, M33, PSR B0540–69

1. INTRODUCTION

While pulsar flux densities are typically quoted as averaged quantities, individual pulses in fact follow a distribution of pulse intensities, with some pulses having intensities of more than 10 times the mean (Hesse & Wielebinski 1974). Many pulsars show approximately normal distributions of pulse intensities about a mean, while some show bimodal distributions, with a finite probability of zero power (e.g. Lyne & Graham-Smith 1998). Other pulsars show asymmetric distributions, with a long tail towards high values of pulse intensity. The Crab pulsar (B0531+21) is an extreme example of this case, with a ‘giant’ pulse more than 10 times the mean intensity occurring once every 1000 pulses (Hankins & Rickett 1975; Lundgren et al. 1995). Such pulses have also been detected from the millisecond pulsars B1821–24 and B1937+21 (Cognard et al. 1996; Romani & Johnston 2001) and, very recently, from the young pulsar B0540–69 (Johnston & Romani 2003). We explore how this giant-pulse phenomenon can be exploited to detect pulsars that may not be detectable through standard periodicity searches. While the main motivation for such a search is the detection of distant, Crab-like pulsars in other galaxies, searches for isolated, dispersed pulses may also be more sensitive than periodicity searches to pulsars seen through the Galactic scattering disk, pulsars with very fast spin periods and pulsars in short binary orbits. There is also the possibility of detecting other classes of radio bursting objects, as discussed in Cordes & McLaughlin (2003) (hereafter Paper I).

In Paper I, we discussed issues related to the detection of fast radio transients from astrophysical sources. We described search algorithms and methodology and in particular discussed the impact of interstellar scintillation and scattering on such searches. In this paper, we apply the methodology of Paper I to searches for giant pulses from extragalactic pulsars. We describe our searches for single radio pulses from M33, PSR B0540–69 in the Large Magellanic Cloud, and several other galaxies. While no giant pulses have been conclusively detected in these searches, we hope that they can serve as blueprints

for future, more sensitive searches for radio transients. Although giant pulses from B0540–69 have recently been detected by Johnston & Romani (2003; hereafter JR03), we present the results of our earlier null search here and discuss the implications of our search for the giant-pulse properties of B0540–69.

The outline of this paper is as follows. In §2, we describe the giant-pulse phenomenon seen in the Crab pulsar and a few others. In §3, we explore the capabilities of single-pulse searches for detecting distant pulsars and compare the sensitivities of single-pulse and standard periodicity searches. In §4, we present results for several targets, including the nearby spiral galaxy M33, B0540–69 and a few other galaxies. Conclusions and a look to the future are offered in §5.

2. THE GIANT-PULSE PHENOMENON

In one hour of observation, the largest measured peak pulse flux of the Crab is roughly $\sim 10^5$ Jy at 430 MHz for a duration of roughly 100 μ s (Hankins & Rickett 1975), corresponding to an implied brightness temperature of 10^{31} K. Recently, pulses with flux $\sim 10^3$ Jy at 5 GHz for a duration of only 2 ns have been detected from the Crab (Hankins et al. 2003). These ‘nano-giant’ pulses imply brightness temperatures of 10^{38} K, by far the most luminous emission from any astronomical object. For many years, this phenomenon was thought to be uniquely characteristic of the Crab. However, giant pulses have since been detected from the Crab-like pulsar B0540–69 and the millisecond pulsars PSRs B1937+21 and B1821–24. For B0540–69, the largest measured peak pulse flux in one hour is approximately 4 Jy (Johnston & Romani 2003). From both millisecond pulsars, the largest measured peak pulse flux in one hour is $\sim 10^3$ Jy at 430 MHz (Cognard et al. 1996; Romani & Johnston 2001).

As shown in Figure 1, the giant pulses detected from the Crab and PSRs B0540–69, B1937+21 and B1821–24 represent the most luminous pulsed emission detected from any pulsar. While PSRs B1937+21 and B1821–24 are ‘recycled’ millisecond pulsars with very different ages, spin periods and surface magnetic field strengths than

¹ Jodrell Bank Observatory, University of Manchester, Macclesfield, Cheshire, SK11 9DL, UK

² Astronomy Department, Cornell University, Ithaca, NY 14853

the Crab and PSR B0540–69, all four pulsars have similarly high values of magnetic field at the light cylinder B_{lc} ($B_{lc} \approx 10^{8.46} P^{-\frac{5}{2}} \dot{P}^{\frac{1}{2}}$ G, where P is pulsar period in seconds and \dot{P} is period derivative). This suggests that giant-pulse physics may depend on conditions there, rather than at the stellar surface. All four pulsars also show high-energy emission at the same phase as their giant pulses, suggesting a relationship between the two phenomena and that the giant-pulse emission process occurs high in the magnetosphere. In Table 1 we list the radio pulsars with the highest values of the magnetic field at the light cylinder.

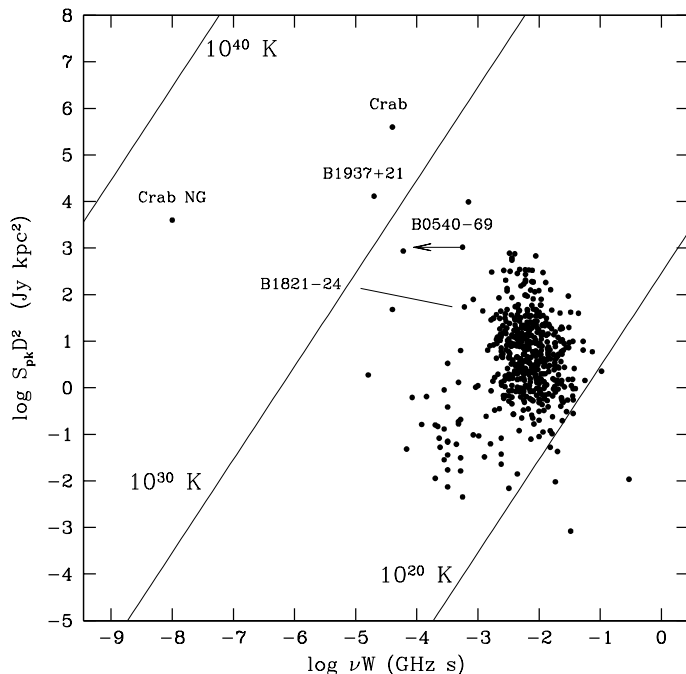


FIG. 1.— A log-log plot of the product of peak flux S in Jy and the square of the distance D in kpc vs. the product of frequency ν in GHz and pulse width W in s for the ‘nano-giant’ pulses detected from the Crab (Hankins et al. 2003), the giant pulses detected from the Crab and PSRs B0540–69, B1937+21 and B1821–24 and single pulses from all pulsars with flux, distance and pulse width listed in the Princeton Pulsar Catalog (Taylor et. al 1993). Lines of constant brightness temperature $T = SD^2/2k(\nu W)^2$ are shown, where k is Boltzmann’s constant.

Lundgren et al. (1995) found that the distribution of Crab pulse fluxes is bimodal, with separate components of the probability distribution function (PDF) describing the normal and giant pulses. As shown in Figure 2, the flux distribution of giant pulses, defined to be those with fluxes exceeding the detection threshold determined by the Crab nebula, can be roughly described by a power law for flux densities above the turnover at ~ 200 Jy. The differential distribution $dN/dS \propto S^{-\alpha}$ with index $\alpha \sim 3.5$. Similarly, the giant-pulse intensity distribution for PSR B1937+21 can be described by a power law of index 2.8 (Cognard et al. 1996). Unlike the Crab’s giant pulses, however, the giant pulses of PSR B1937+21 appear to be the extreme of a continuous distribution of pulse intensities. The giant pulses of PSR B1821–24 are less well-studied but seem to be adequately described by a power law of index 3 – 5 (Romani & Johnston 2001). Too few pulses have been detected from PSR B0540–69 to constrain their flux

density distribution (Johnston & Romani 2003).

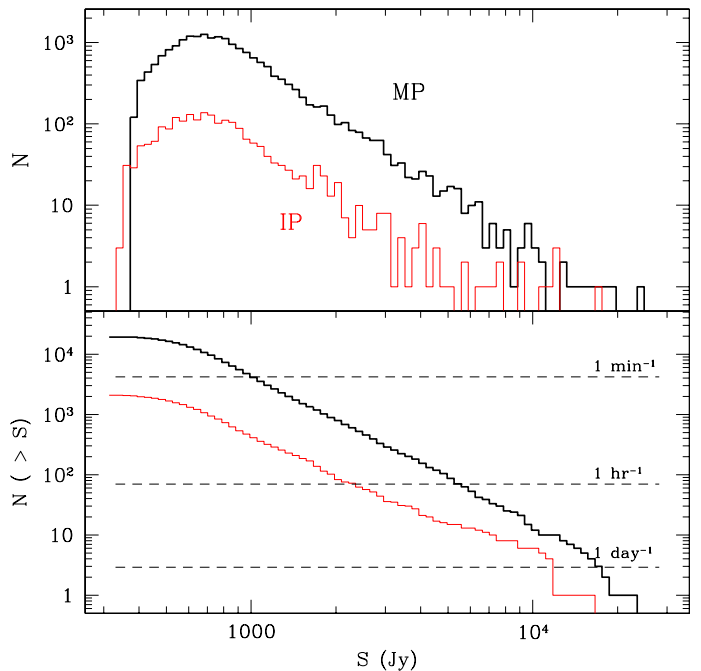


FIG. 2.— Peak flux densities of giant pulses from the Crab pulsar. The upper panel shows results obtained from 70 hours of observation at 812 MHz with the 140-ft telescope at Green Bank (Lundgren et al. 1995). Histograms are shown separately for the main pulse (MP) and interpulse (IP) components. The flux scale is different from that in Lundgren et al. because their Figure 4 gives the flux integrated over a window that is 1.5 ms wide. We have converted to peak flux densities by assuming the typical pulse width of 100 μ s inferred by Lundgren et al. The lower panel shows the corresponding cumulative distributions, with dashed lines marking detection rates of one pulse per minute, one pulse per hour and one pulse per day.

3. DETECTABILITY OF GIANT PULSES

The vast majority of the over 1500 radio pulsars known were discovered through searches for periodic signals using Fourier methods. Because these searches incorporate many pulses from a single source, they are generally more sensitive than single-pulse searches. However, there are some conditions under which a single-pulse search may be more sensitive than a search for periodicity. In this section, we describe how searches for single pulses may be more effective than periodicity searches at detecting distant, giant-pulse emitting pulsars.

Finding distant pulsars in other galaxies is important as, of the roughly 1500 radio pulsars known, only ~ 25 are extragalactic, all located in the Magellanic Clouds (A. G. Lyne, personal communication). Detection of extragalactic pulsars would allow us to study pulsar populations in other galaxies and to probe the interstellar medium in those galaxies as well as the intervening intergalactic medium. Finding more young pulsars like the Crab is crucial for understanding neutron star formation, supernovae and the early stages of pulsar evolution. However, Crab-like pulsars in our Galaxy are difficult to detect due to propagation processes, particularly scattering, through the Galactic plane. Searching for extragalactic pulsars is attractive because such searches may not suffer as greatly from such effects. We show

how giant-pulse searches may be the most effective way of detecting these distant pulsars and use the properties of the Crab pulsar to infer to what distances we would be able to detect similar pulsars in other galaxies. We also compare the efficacy of searches for single pulses with that of traditional periodicity searches.

From the radiometer equation, we calculate the maximum distance to which a giant pulse like those observed from the Crab pulsar could be detected. Following the notation of §3.4 of Paper I and assuming matched filtering to a pulse that is temporally resolved, the maximum detectable distance scales with the Crab Nebula's distance $D_C = 2$ kpc as

$$\begin{aligned}
 D_{\max} &= S/N_{\min}^{-1/2} D_C \left(\frac{S_{\text{GP}}}{S_{\text{sys}}} \right)^{1/2} (N_{\text{pol}} \Delta\nu W)^{1/4} \\
 &\approx 0.85 \text{ Mpc} \left(\frac{S/N_{\min}}{5} \right)^{-\frac{1}{2}} \left(\frac{S_{\text{sys}}}{5 \text{ Jy}^{-1}} \right)^{-\frac{1}{2}} \left(\frac{S_{\text{GP}}}{10^5 \text{ Jy}} \right)^{\frac{1}{2}} \\
 &\quad \times \left[\left(\frac{\Delta\nu}{10 \text{ MHz}} \right) \left(\frac{W}{0.1 \text{ ms}} \right) \left(\frac{N_{\text{pol}}}{2} \right) \right]^{\frac{1}{4}} \quad (1)
 \end{aligned}$$

where S/N_{\min} is the S/N threshold, $S_{\text{sys}} = T_{\text{sys}}/G$ is the system noise in Jansky units (system temperature divided by the telescope gain), $\Delta\nu$ is the receiver bandwidth, W is the pulse width, assumed larger than the post-detection time constant, or sampling interval, τ , N_{pol} is the number of independent polarization channels summed and S_{max} is the peak flux density of the giant pulse in the time of observation. We have assumed in deriving Eq. 1 that pulses are dedispersed and that any residual pulse smearing (e.g. from scattering) is less than W . Using fiducial values for an Arecibo 430-MHz search ($\Delta\nu = 10$ MHz, $N_{\text{pol}} = 2$, $W \sim 0.1$ ms, $S_{\text{sys}} = 5$ Jy), and a threshold $S/N_{\min} = 5$, we calculate $D_{\max} \sim 0.85$ Mpc for Crab-like pulsars in a one-hour observation (i.e. $S_{\text{max}} \sim 10^5$ Jy). For millisecond pulsars like PSR B1937+21 ($D = 3.6$ kpc) and PSR B1821-24 ($D \approx 5.5$ kpc) for which $S_{\text{max}} \sim 10^3$ Jy in one hour, $D_{\max} \sim 0.15$ to 0.23 Mpc.

Given the distribution of giant-pulse intensities measured by Lundgren et al. (1995), we calculate the number of Crab-like giant pulses detectable out to a distance D_{\max} in such a search. As shown in Figure 3, Crab-like pulsars within several irregular and spiral galaxies in the Local Group, at distances less than 1 Mpc, would be detectable at rates greater than one pulse per hour. These include the LMC, SMC, M31, M33, NGC6822 and IC1613. If giant pulses an order of magnitude greater than the Crab's are emitted, then another 7 galaxies in the 2 to 4.3 Mpc range, including M81, M82, M83, M94, M63, M51 and M101, might be accessible. Making the naive assumption that all pulsars of the Crab's age (~ 1000 yr) or less will emit giant pulses, and assuming a pulsar birthrate of 1 per 100 years, we estimate that at least 10 giant-pulse emitting pulsars should be within each spiral galaxy similar to our own. Searching for these young pulsars is attractive as such searches may not be as impeded by dispersion and scattering as are searches for pulsars within our own galaxy.

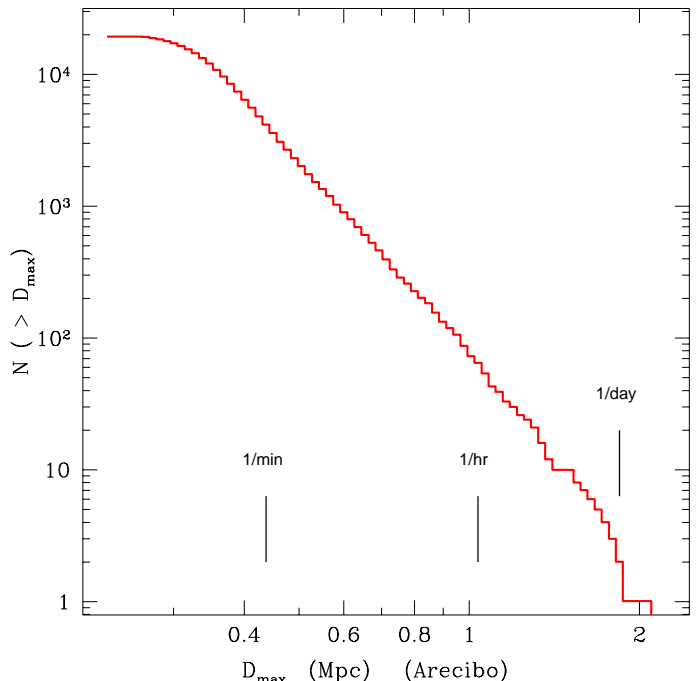


FIG. 3.— Number of detectable Crab-like giant pulses out to a distance D_{\max} for a 70-hr Arecibo search at 430 MHz with bandwidth of 10 MHz, a 5σ detection threshold and matched filtering (c.f. Eq. 1). We have scaled the distribution of pulse amplitudes at 812 MHz from Lundgren et al. (1995) by assuming a spectral index of -4.5 for giant pulses. This spectral index is consistent with the work of Sallmen et al. (1999). Also, the predicted rate of detections is consistent with recent Crab pulsar observations we have made (Cordes et al. 2003) at 430 MHz which yield $S_{\text{max}} = 1.6 \times 10^5$ Jy in one hour of observing and imply $D_{\max} = 1.6$ Mpc.

It is useful to compare single-pulse and periodicity searches and the resultant maximum distances to which an isolated pulsar would be detectable through the two methods. Letting $D_{\max, \text{SP}}$ and $D_{\max, \text{FFT}}$ be the maximum distances to which we could detect a pulsar through a search for single pulses and through a FFT-based standard periodicity search, their ratio,

$$\frac{D_{\max, \text{SP}}}{D_{\max, \text{FFT}}} = \left(\frac{S/N_{\min}(\text{FFT})}{S/N_{\min}(\text{SP})} \right)^{\frac{1}{2}} \left(\frac{S_{\text{max}}}{S_{\text{avg}}} \right)^{\frac{1}{2}} \left(\frac{\tau}{T} \right)^{\frac{1}{4}} \left(\frac{W}{P} \right)^{\frac{1}{4}}, \quad (2)$$

depends on the thresholds for the periodicity and single-pulse searches $S/N_{\min}(\text{FFT})$ and $S/N_{\min}(\text{SP})$, the post-detection time constant τ (optimally equal to the pulse width W), the total time integrated T , the maximum pulse giant pulse flux density, S_{max} , seen in that time, the average flux S_{avg} , and the period of the pulsar P . For typical parameters ($S/N_{\min}(\text{SP}) = 5$, $S/N_{\min}(\text{FFT}) = 8$, $T = 3600$ s, $\tau = 0.1$ ms and $W/P = 0.05$), we find that a search for single pulses can detect pulsars to greater distances than the periodicity search when $S_{\text{max}}/S_{\text{avg}} > 1.7 \times 10^4$. The Crab pulsar, with $S_{\text{max}}/S_{\text{avg}} = 1.5 \times 10^5$ satisfies this criterion while PSR B1937+21, with $S_{\text{max}}/S_{\text{avg}} = 4.2 \times 10^3$, does not.

A more detailed analysis in the Appendix compares the two methods for different pulse-amplitude distributions. For distributions that are strictly power-law in form and with a large range of pulse amplitudes, single pulse searches are superior to periodicity searches for power-law indices α in the range of $1 \lesssim \alpha \lesssim 3$ when the number of

pulse periods investigated ranges from ~ 10 to 10^5 . For the Crab pulsar, $\alpha \approx 3.5$, but single-pulse detection is superior to a periodicity search because pulses comprise both a power-law distribution and a component of much weaker but more frequent pulses. We find that in some circumstances, single-pulse searches are more effective than searches for periodicity, *even in the absence of giant pulses*. These regimes are further outlined in the Appendix and show that pulsar searches should always incorporate single-pulse searches in addition to standard periodicity searches. The computational time needed for the single-pulse search is typically a small fraction ($< 10\%$) of the total search time. We note that the relative sensitivities of single-pulse and periodicity searches will depend on the extent and nature of radio frequency interference (RFI), with single-pulse searches being more affected by bursty, aperiodic RFI.

4. SEARCHES FOR EXTRAGALACTIC PULSARS

We now describe the results of searches for giant pulses from the nearby spiral galaxy M33, PSR B0540–69 in the LMC and from several other galaxies. While these searches were designed to detect giant pulses from pulsars, they are sensitive to other transient radio sources and serve as practical examples of applying the methodology described in Paper I. They also illustrate the challenges of searches for fast radio transients in the presence of RFI.

4.1. M33

As shown in Figure 3, all of the galaxies in the Local Group are within the range of detection of Crab-like giant pulses. The spiral galaxy M33, at a distance of approximately 840 kpc (Freedman et al. 1991; Freedman et al. 2001), is an excellent candidate for giant-pulse detection because its light derives mainly from blue, supergiant stars (i.e. progenitors of neutron stars). It is also visible with Arecibo, currently the most sensitive instrument for single-pulse searches at \sim meter wavelengths. Our Arecibo search used a radio frequency of 430 MHz, optimal because of the steep spectral indices of pulsars and the low dispersion and scattering expected towards M33. The entire galaxy was covered with $16 \times 9'$ -diameter beams, as shown in Figure 4. In Table 2 we list beam number, RA and DEC in J2000 coordinates, the number of pointings at each beam and the total observation time per beam. Each beam was observed five to ten times for 900 or 1800 seconds over MJDs from 51054 to 52406 (i.e. from 29 August 1998 to 12 May 2002). The total amount of time spent per beam over these dates ranged from 1.75 to 3.0 hours. Two off-source positions were also observed, to provide an independent test of the reality of any detected signals. Observations were done with the Arecibo Observatory Fourier Transform Machine (AOFTM, <http://www.naic.edu/~aoftm/>), which covers a 10-MHz bandwidth with 1024 frequency channels and uses a sampling time of 102.4 μ s.

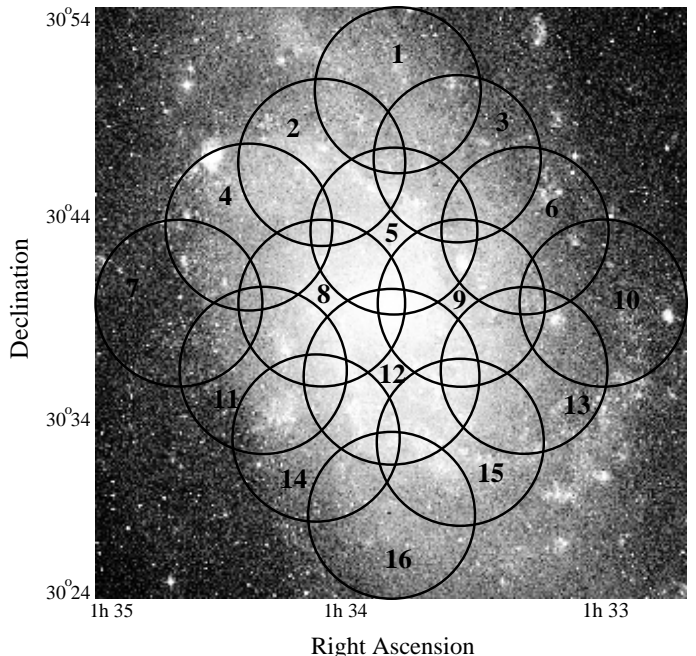


FIG. 4.— The sixteen beams used for our Arecibo giant-pulse search superposed on an image of M33 from the Digitized Sky Survey (York et al. 2000). Gordon et al (1999) have cataloged 53 radio-bright supernova remnants in M33, the largest extragalactic sample ever. These remnants are fairly uniformly spaced out to a distance of roughly 15 arcminutes from the center of the galaxy, with the most distant remnant lying approximately 20 arcminutes from the center. There are a total of 98 cataloged supernova remnants in M33, compared with 231 in our Galaxy (Green 2002).

Due to the high latitude ($|b| \sim 30^\circ$) of M33, the predicted Galactic contribution to the dispersion measure (DM) along the line of sight is only $\sim 50 \text{ pc cm}^{-3}$ (Cordes & Lazio 2002). As the orientation of M33 is nearly face-on (Garcia-Gomez & Athanassoula 1991), we take Galactic and extragalactic DM contributions to be equal and estimate the maximum dispersion smearing expected across a 10-kHz frequency channel to be $\sim 0.1 \text{ ms}$. To allow for errors in the model and any regions of enhanced electron density along the line of sight, our searched DMs ranged from 0 pc cm^{-3} to 250 pc cm^{-3} . Scaling from the Green Bank measurements of Lundgren et al. (1995), as in Figure 3, we estimate that more than one pulse per hour should be detectable from a Crab-like pulsar in M33 above a S/N threshold of 5, corresponding to a threshold of 0.5 Jy. Assuming a pulsar birthrate of 0.01 yr^{-1} , we expect there to be roughly 10 pulsars of the Crab’s age or less in our Galaxy. Because the mass of M33 is roughly 10 times less than that of our Galaxy (Méndez et al. 1999; Corbelli & Salucci 2000; Sakamoto et al. 2003), we might expect 10 times fewer young, Crab-like pulsars. However, evidence suggests that the supernova rate per unit mass is higher in M33 than in our Galaxy (Berkhuijsen 1984; Gordon et al. 1998). Because these mass and supernova rate estimates are highly uncertain, it is difficult to predict how many Crab-like pulsars there might be in M33, but we expect it to be of order ~ 10 . Furthermore, since giant pulses are also emitted by millisecond pulsars like PSRs B1821–24 and B1937+21, the number of detectable pulsars may be larger.

Because RFI contaminated much of our data, our

actual threshold was often significantly higher than that calculated from radiometer noise alone. In some cases, RFI was minor and did not greatly influence our sensitivity to pulses of astrophysical origin. In other cases, however, the RFI was quite strong and significant portions of the data had to be discarded from the analysis. This was done with interactive tools for displaying and selecting subsets of data in time and DM space.

For each beam, we applied the search algorithms described in Paper I to create diagnostic plots like those shown in Figures 5, 6 and 7 and inspected the results for evidence of high-DM pulses of an astrophysical origin. In Paper I similar plots for the giant-pulsing pulsars PSRs B0531+21 and B1937+21 are shown. For our M33 search, a signal-to-noise threshold of 4 was used and each time series was smoothed in seven stages (where adjacent samples were summed in each stage), corresponding to a maximum time resolution of $2^7 \times 102.4 \mu\text{s} \approx 13$ ms. If a pulse is detected in several of the smoothed time series, only the highest S/N pulse is recorded. Most beams, like that shown in Figure 5, show an excess of pulses at low DM due to RFI but show no evidence for high DM pulses. For some beams, the most dramatic example of which is shown in Figure 6, we detect an excess number of pulses at a well-defined, non-zero DM. For other beams, as shown in Figure 7, we detect individual strong pulses at high DM. While these features are tantalizing and, in some cases, consistent with originating from a pulsar in M33, no features repeat on multiple pointings at the same position. However, this is not inconsistent with the predictions of Figure 3. For each beam, we summed all of the DM histograms (i.e. upper right panels of Figures 5, 6 and 7) to determine if low-level excesses of pulses at a specific DM were present. However, no features were apparent in these combined histograms.

It is unlikely that interstellar scintillation is responsible for features, such as those shown in Figures 6 and 7, appearing only sporadically. Assuming a Galactic scale height of 1 kpc for C_n^2 (the electron-density fluctuation spectral coefficient; see Paper I) and a source velocity of 200 km/s (e.g. Arzoumanian et al. 2002) and applying the results of the Appendix of Paper I, we find that a source in M33 should have a scintillation timescale of only ~ 35 seconds and a scintillation bandwidth of only ~ 20 kHz at 430 MHz, rendering ISS unimportant in modulating source intensities during or between our observations. At 1400 MHz, these timescales and bandwidths would be much larger (roughly 141 seconds and 3.6 MHz) and would be important to consider.

Unfortunately, for the time being, our search for giant pulses from M33 pulsars remains inconclusive. It could be that the Crab and PSR B0540–69 are unusual pulsars and that there are no similar, giant-pulse emitting pulsars in M33. It is also possible that we have detected giant pulses from M33 pulsars, but they are either too sporadic or too weak to be distinguished from the many pulses due to RFI. Sensitive, multiple-beam and/or multiple-site observations are necessary to conclusively assess the reality of the signals we have detected.

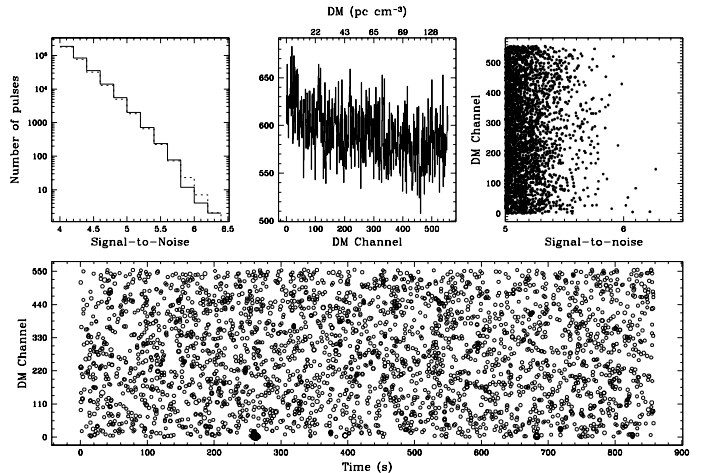


FIG. 5.— Single-pulse search results for M33 beam 4 on MJD 52405. UPPER LEFT: The number of pulses above a 4σ threshold vs. signal-to-noise. Note the logarithmic scale of the y-axis. The dotted line shows the expected distribution for noise only, as described in Paper I. UPPER CENTER: Number of pulses above a 4σ threshold vs. DM channel. The lower x-axis shows DM channel number, while the upper x-axis shows DM in pc cm^{-3} . We have used the optimal DM channel spacing described in Section 3.2 of Paper I. UPPER RIGHT: DM channel vs signal-to-noise for all pulses with S/N greater than 5σ . To create these three upper plots, pulses which are strongest at zero DM have been excised. BOTTOM: All pulses with signal-to-noises greater than 5σ plotted vs. DM channel and time. The size of the circle is linearly proportional to the signal-to-noise of the pulse. Even though we ignore them in our analysis, pulses which are strongest at low DM are shown in this bottom plot to illustrate the effects of RFI. As for the majority of M33 observations, there are no strong individual pulses at high DM. Likewise, an excess of pulses at high DM in the DM histogram is not apparent.

In addition to the single-pulse search, a periodicity search was performed on all of the M33 data, typically using 8-Mpoint FFTs (i.e. roughly 14 minutes of data at our $102.4 \mu\text{s}$ sampling rate). While the chances of detecting a pulsar in M33 through such a search are very small (the pulsar would have to have an average flux density of approximately 30 times that of the Crab's), we were sensitive to pulsars within our own Galaxy along the

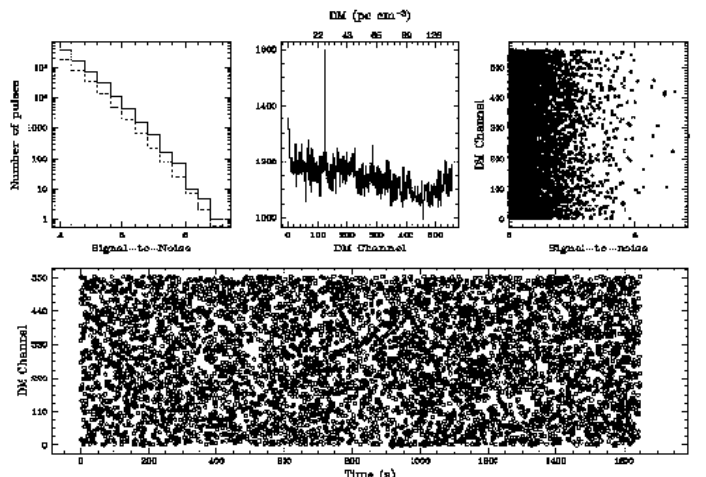


FIG. 6.— Single-pulse search results for M33 beam 13 on MJD 51918. An excess of single pulses at $\text{DM} \sim 26.5 \text{ pc cm}^{-3}$ is obvious. This excess is due to many weak pulses; no strong single pulses at this DM are seen. This pulse must have width < 0.1 ms to show such a narrow DM distribution (see Figures 3 and 4 of Paper I).

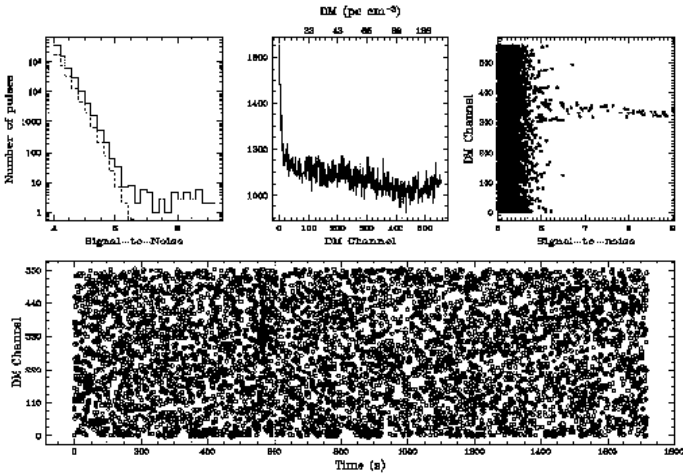


FIG. 7.— Single-pulse search results for M33 beam 16 on MJD 51921. In addition to an excess of pulses at zero DM due to RFI, a small excess of pulses is detected at the DM of this

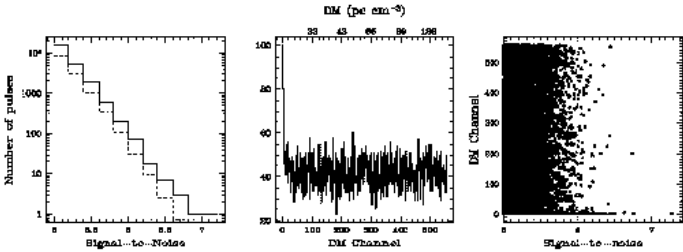


FIG. 8.— Single-pulse search results for pointings away from M33. These plots show cumulative results for all pulses above 5σ for all five 1800-second off-source datasets. No strong individual pulses or excesses in the DM histogram are detected.

4.2. PSR B0540–69

With a period of 50.3 ms, a period derivative of $4.8 \times 10^{-13} \text{ s s}^{-1}$, and hence a spin-down age of roughly 1660 years, pulsar B0540–69 has more similar spin-down parameters to the Crab pulsar than any other known pulsar. Furthermore, as shown in Table 1, the magnetic field at the light cylinder of this pulsar, the strength of which seems to be correlated with giant-pulse emission, is fifth among known radio pulsars. Although it is roughly 50 kpc away in the LMC, it is a strong X-ray and optical source. The DM of PSR B0540–69 measured by Manchester et al. (1993) is $146 \pm 4 \text{ pc cm}^{-3}$. They measure a 640 MHz flux of 0.4 mJy, roughly the same flux that the Crab would have at the distance of the LMC. While its integrated radio emission is weak, we might expect PSR B0540–69 to emit giant pulses similar to those detected from the Crab. The detection of such pulses from PSR B0540–69 would allow us to compare the shapes and phases of giant pulses with those at high energies, determine the dispersion measure more accurately and perhaps measure polarization of strong giant pulses.

With this in mind, we obtained a total of 55 observations of PSR B0540–69 between September 7, 1994 and September 26, 1994 with the Parkes Radiotelescope in New South Wales, Australia. These include 15 observations at a center frequency of 660 MHz, with 256 0.125-MHz channels covering a 32-MHz bandpass, and

40 observations at a center frequency of 1520 MHz, with 64 5-MHz channels covering a 320-MHz bandpass. At both frequencies, a sampling time of 0.6 ms was used. Most of our pointings were one-hr long, bringing the total number of hours on source to 14.4 hours at 660 MHz and 38.1 hours at 1520 MHz. Our 5σ single-pulse detection thresholds calculated from radiometer noise were 4 Jy and 0.5 Jy at 660 and 1520 MHz, respectively. Actual thresholds were significantly higher in some pointings due to RFI, but most RFI could be excised by discarding subsets of the data from the analysis.

Given the parameters above, we would expect to detect Crab-like giant pulses up to S/Ns of 9 and 17 at the lower and upper frequencies, respectively, in our total observation times at the two frequencies (assuming a spectral index of -2). In Figures 9 and 10, we plot the signal-to-noises and DMs of all pulses detected above a 5σ threshold at both frequencies. Our data at 660 MHz do not show any evidence for giant pulses at the DM of B0540–69. At 1520 MHz, the strongest non-zero DM pulse has an amplitude of 7σ and a DM of 146 pc cm^{-3} . While this is tantalizing, several pulsars nearly as strong are detected at other DMs, and we cannot claim detection of giant pulses with our data. Given the large scattering timescales measured by JR03, it is unlikely that scintillation played a role in modulating the fluxes of pulses during our observation.

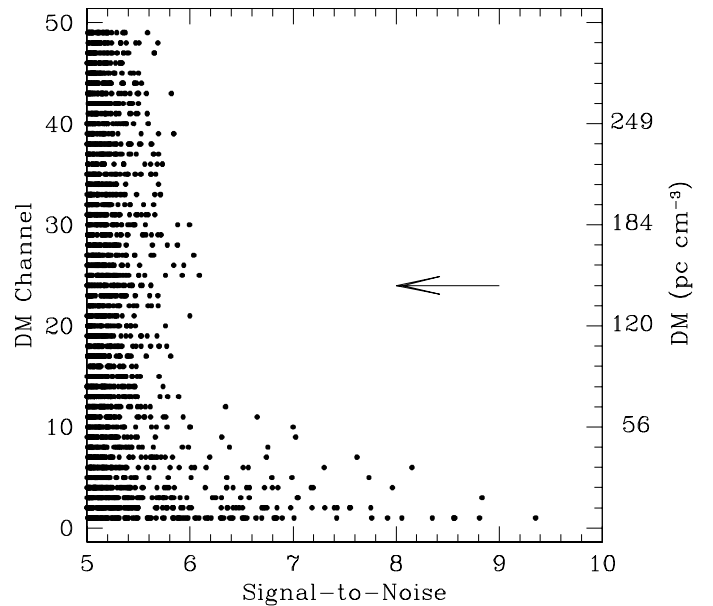


FIG. 9.— DM vs. signal-to-noise for all pulses detected above a threshold of 5σ from PSR B0540–69 at a center frequency of 660 MHz. The arrow shows the pulsar’s DM of 146 pc cm^{-3} .

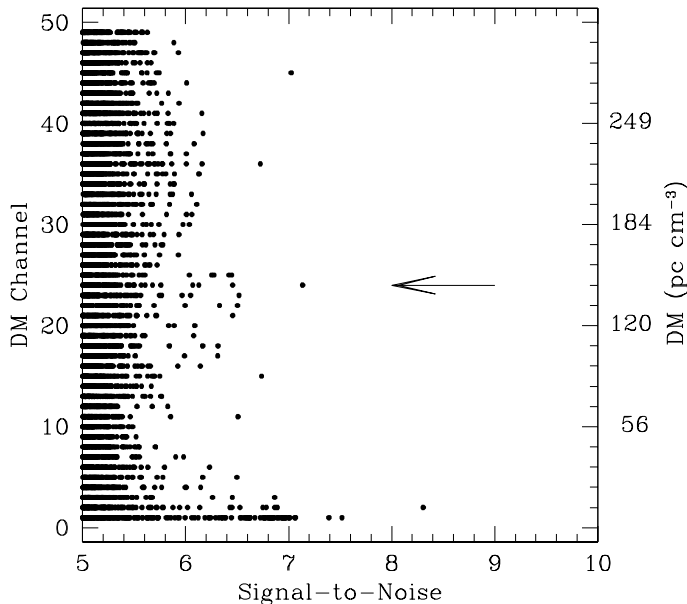


FIG. 10.— DM vs. signal-to-noise for all pulses detected above a threshold of 5σ from PSR B0540-69 at a center frequency of 1520 MHz. The arrow shows the pulsar’s DM of 146 pc cm^{-3} .

While the 1384-MHz JR03 observations benefited from a new Parkes receiver with lower system temperature and a slightly lower observing frequency, the main difference between their observations and the observations reported here is the channel bandwidth. They used 0.5-MHz filters, implying smearing of only $230 \mu\text{s}$ for a DM of 146 pc cm^{-3} . Our 5-MHz filters caused a DM smearing of 1.8 ms, much more than the scatter-broadened giant-pulse width of 0.4 ms measured by JR03. Given the peak giant-pulse fluxes and widths reported by JR03, we would expect to detect their strongest pulse at a signal-to-noise of 8σ . Adding in the effects of a slightly higher observing frequency and increased system noise, the pulse signal-to-noise distribution in Figure 10 is consistent with their observations.

Our non-detection of giant pulses at 660 MHz is more difficult to understand. Given the 0.4-ms scatter-broadened width of the pulses detected by JR03, we expect 10-ms of scatter broadening at 660 MHz, much greater than the 0.5-ms expected DM smearing across one of our 0.125-MHz channels. If the spectral index of PSR B0540-69 is indeed as steep as -4.4 , as the observations by JR03 suggest, we would expect to detect pulses as strong as 20σ in our data. A spectral index of -3 or higher is required to explain our null results at 660 MHz.

4.3. Other Galaxies

During our search for giant pulses from PSR B0540-69, we observed several other galaxies. While it is unlikely that a pulsar could be detected in any of these galaxies, aside from the LMC, these searches are constraining for some of the other source populations discussed in Section 2 of Paper I. In Table 3, we list these targets, along with Right Ascension, Declination, Galactic longitude, Galactic latitude, estimated distance and the number of pointings N_p at each object. Each pointing was 1800-seconds long and for most pointings we used a central frequency of

435 MHz, with 256 channels of width 0.125-MHz and a sampling time of 0.42 ms. Galaxies NGC253, NGC300, Fornax, NGC6300 and NGC7793 were all covered by a single Parkes beam, while 6 separate pointings were necessary to cover the 2 deg^2 error box of the high-energy LMC source 3EG J0533-69 (Hartman et al. 1999). We performed a search for single pulses on all of the pointings, but did not find any conclusive evidence for isolated dispersed pulses from any of these galaxies. In Figure 11, we present results for the LMC pointing with the 16-ms X-ray pulsar J0537-6910 in the beam. This pulsar is interesting as it has a B_{lc} which is over twice that of the Crab or PSR B1937+21. We detect an excess of pulses at a DM of 113 pc cm^{-3} , consistent with the DMs of pulsars already detected in the LMC (Crawford et al. 2001). However, because of the presence of RFI which manifests itself as dispersed radio pulses at many DMs, it is impossible to assess the reality of this signature. More sensitive and/or multiple beam/multiple site observations are required.

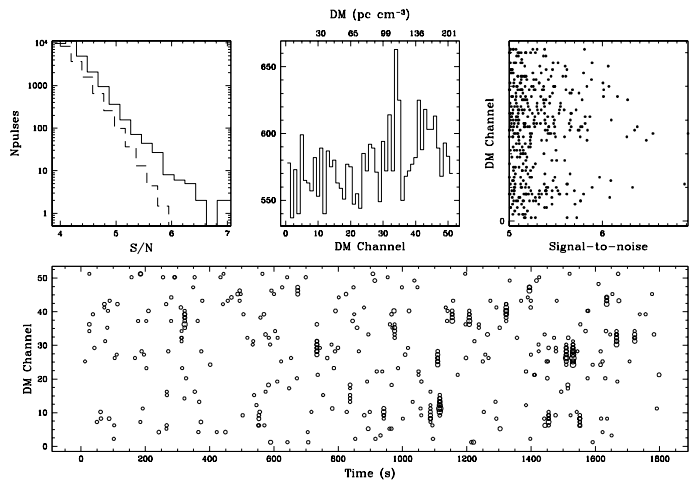


FIG. 11.— Single-pulse search results for the 1800-second LMC pointing at 435 MHz with the 16-ms X-ray pulsar J0537-6910 in the beam. While an excess number of pulses is detected at a DM $\sim 113 \text{ pc cm}^{-3}$, strong pulses across many DMs due to RFI make assessing the reality of this excess difficult.

5. CONCLUSIONS

We have described the capabilities of searches for extragalactic giant pulses and the results of several searches towards extragalactic targets. We find that giant pulses from Crab-like pulsars should be detectable from all galaxies in the Local Group. We explore different pulse-amplitude power distributions and intensity cutoffs and find that single-pulse searches are superior to periodicity searches in certain cases. We emphasize that this kind of search should be done along with standard periodicity searches for pulsars because of the small additional computational efforts and the possibly large gains. The example results from searches for giant pulses from extragalactic pulsars illustrate the methodology and challenges of any search for transient radio signals. We have detected several intriguing dispersed pulses of possibly astrophysical origin from the spiral galaxy M33 with a search using the Arecibo radiotelescope at 430 MHz. Assessment of the astrophysical nature of these pulses must wait for more sensitive multiple-beam and/or

multiple-site observing systems. We have detected no convincing signatures of giant pulses from the young LMC pulsar B0540–69 or from several other galaxies in searches with the Parkes radio telescope.

While the results of the M33 search presented here are inconclusive, they illustrate both the capabilities and difficulties in single-pulse searches and serve as a pilot study for future searches. To increase the capabilities of single-pulse searches, systems with multiple beams or multiple antennas are necessary in order to perform coincidence tests which will discriminate between pulses of astrophysical and terrestrial origins. Larger collecting areas are needed to increase our sensitivity to pulses from pulsars and other transient sources in other galaxies. Multi-beam systems for the Arecibo and Green Bank telescopes will likely be built within the next few years. Observing with multiple beams will allow us to distinguish RFI from real signals and would remove much of the ambiguity in interpreting the results of our M33 search. On a longer time scale, large radio arrays such as the

Square Kilometer Array (SKA) will be developed. With a planned field of view over 100 times that of Arecibo and a sensitivity over 20 times that of Arecibo, the SKA will revolutionize single-pulse searches. While the SKA will not be operational for many years, single-pulse searches in the meantime, especially with multiple beams, are essential for optimizing routines for RFI excision and for processing large amounts of data.

We thank Simon Johnston and Froyen Crawford for useful discussions. MAM is supported by an NSF Math and Physical Sciences Distinguished Research Fellowship. Arecibo Observatory is operated by the National Astronomy and Ionosphere Center, which is operated by Cornell University under cooperative agreement with the National Science Foundation (NSF). The Parkes Observatory is part of the Australia Telescope which is funded by the Commonwealth of Australia for operation as a National Facility managed by CSIRO.

REFERENCES

- Arzoumanian, Z., Chernoff, D. F., & Cordes, J. M. 2002, *ApJ*, 568, 289
- Berkhuijsen, E. M. 1984, *A&A*, 140, 431
- Burns, W. R. & Clark, B. G. 1969, *A&A*, 2, 280
- Camilo, F. et al. 2002, *ApJ*, 571, L41
- Cognard, I., Shrauner, J. A., Taylor, J. H., & Thorsett, S. E. 1996, *ApJ*, 457, L81
- Corbelli, E. & Salucci, P. 2000, *MNRAS*, 311, 441
- Cordes, J. M. & Lazio, T. J. W. L. 2002, astro-ph/0207156
- Cordes, J. M. & McLaughlin, M. A. 2003, *ApJ*, submitted
- Crawford, F., Kaspi, V. M., Manchester, R. N., Lyne, A. G., Camilo, F., & D’Amico, N. 2001, *ApJ*, 553, 367
- Freedman, W. L., Wilson, C. D., & Madore, B. F. 1991, *ApJ*, 372, 455
- Freedman, W. L. et al. 2001, *ApJ*, 553, 47
- Garcia-Gomez, C. & Athanassoula, E. 1991, *A&AS*, 89, 159
- Gordon, S. M., Kirshner, R. P., Long, K. S., Blair, W. P., Duric, N., & Smith, R. C. 1998, *ApJS*, 117, 89
- Gordon, S. M., Duric, N., Kirshner, R. P., Goss, W. M., & Viallefond, F. 1999, *ApJS*, 120, 247
- Green, D. A. 2002, *VizieR Online Data Catalog*, 7227
- Hartman, R. C., et al., 1999, *ApJS*, 123, 79
- Hankins, T. H. & Rickett, B. J. 1975, *Methods in Computational Physics*. Volume 14 - Radio astronomy, 14, 55
- Hankins, T. H., Kern, J. S., Weatherall, J. C., & Eilek, J. A. 2003, *Nature*, 422, 141
- Hesse, K. H. & Wielebinski, R. 1974, *A&A*, 31, 409
- Hewish, A., Bell-Burnell, J., Pilkington, J. D. H., Scott, P. F., & Collins, R. A. 1968, *Nature*, 217, 709
- Johnston, S. & Romani, R. W. 2003, submitted to *ApJ*
- Lundgren, S. C. et al. 1995, *ApJ*, 453, 433
- Manchester, R. N., et al., 1993, *ApJ*, 403, L29
- Méndez, R. A., Platais, I., Girard, T. M., Kozhurina-Platais, V., & van Altena, W. F. 1999, *ApJ*, 524, L39
- Romani, R. W. & Johnston, S. 2001, *ApJ*, 557, L93
- Sakamoto, T., Chiba, M., & Beers, T. C. 2003, *A&A*, 397, 899
- Sallmen, S., Backer, D. C., Hankins, T. H., Moffett, D., & Lundgren, S. 1999, *ApJ*, 517, 460
- Staelin, D. H. & Reifenstein, E. C., 1968, *Science*, 162, 1481
- Taylor, J. H., Manchester, R. N., & Lyne, A. G., 1993, *ApJS*, 88, 529
- York, D. G. et al. 2000, *AJ*, 120, 1579

APPENDIX

PERIODICITY SEARCHES VS. SINGLE-PULSE SEARCHES

This appendix considers the detectability of pulsars with respect to two broad search techniques: one that exploits the inherent periodicity and another that identifies individual, large-amplitude pulses. Burns & Clark (1969) made a brief comparison of these techniques but, for the most part, pulsar astronomers have relied on periodicity searches. Consider a time interval of length T in which there are N_p pulse periods. Pulse intensity maxima are described by a continuous probability density function (PDF) $f_S(S)$ and its integral, the cumulative distribution function (CDF) $F_S(S)$.

Single-Pulse Search Detection

Given system noise S_{sys} expressed in Janskys, the signal-to-noise ratio (S/N) of the pulse peak S_{max} in the sum of N_{pol} polarization channels when the pulse is match filtered is

$$(S/N)_{\text{SP}} = \eta(N_{\text{pol}}\Delta\nu W)^{1/2} S_{\text{sys}}^{-1} S_{\text{max}}, \quad (\text{A1})$$

where $\eta \sim 1$ is a pulse-shape-dependent factor, $\Delta\nu$ is the total bandwidth and W is the pulse width. For a Gaussian pulse shape, $\eta = (\pi/8 \ln 2)^{1/4} \approx 0.868$. Single pulse detection would entail specifying some threshold S/N of at least 3 and probably much larger, depending on how many statistical trials were made in a survey.

For PDFs with long tails, one should take into account the fact that f_S is truncated at the maximum likely intensity in the interval. Assuming that all pulses have the same width W , we define the maximum pulse intensity likely to occur in the interval from the constraint $[1 - F_S(S_{\text{max}})]N_p = 1$, implying

$$F_S(S_{\text{max}}) = 1 - N_p^{-1}. \quad (\text{A2})$$

Periodicity Search Detection

In a search for a periodic signal in the time series, the Fourier analysis effectively measures the period-averaged mean intensity for the time interval. The period-averaged intensity is defined to be $\langle S \rangle_\phi = \zeta(W/P)S_{\text{avg}}$, where S_{avg} is the mean *peak* intensity, ζ is a shape-dependent constant ~ 1 and P is the pulse period. For a Gaussian pulse with FWHM W , $\zeta = \sqrt{\pi/\ln 2}/2 \approx 1.06$. In terms of the pulse-peak PDF, the ensemble mean of the peak intensity is

$$S_{\text{avg}} \equiv \int dS S f_S(S). \quad (\text{A3})$$

However, recognizing that PDFs with long tails yield a maximum intensity in a finite number of pulse periods, we define a modified mean intensity,

$$S'_{\text{avg}} = \frac{\int_0^{S_{\text{max}}} dS S f_S(S)}{\int_0^{S_{\text{max}}} dS f_S(S)} = (1 - N_p^{-1})^{-1} \int_0^{S_{\text{max}}} dS S f_S(S). \quad (\text{A4})$$

The S/N for a periodicity search over an interval $T \equiv N_p P$ is

$$(S/N)_{\text{FFT}} = (N_{\text{pol}}\Delta\nu T)^{1/2} S_{\text{sys}}^{-1} \langle S \rangle_\phi h_\Sigma, \quad (\text{A5})$$

where the harmonic sum is

$$h_\Sigma = N_h^{-1/2} \sum_{\ell=1}^{N_h} R_\ell, \quad (\text{A6})$$

with R_ℓ equal to the ratio of the ℓ -th harmonic's Fourier amplitude to that of the DC value. The leading factor $N_h^{-1/2}$ takes into account that the threshold increases as the number of harmonics summed increases. For a Gaussian pulse shape,

$$R_\ell = \exp \left[- \left(\frac{\pi W \ell}{2P\sqrt{\ln 2}} \right)^2 \right], \quad (\text{A7})$$

and the number of harmonics maximizing h_Σ is $N_{h_{\text{max}}} \approx P/2W$. The value of the harmonic sum at the maximum is well approximated by $h_{\Sigma_{\text{max}}} \approx 1/2 (P/W)^{1/2}$. The S/N of the periodicity search using the harmonic sum is then

$$(S/N)_{\text{FFT}} = (\zeta/2)(N_{\text{pol}}\Delta\nu W)^{1/2} S_{\text{sys}}^{-1} N_p^{1/2} S'_{\text{avg}}. \quad (\text{A8})$$

Comparing Single-Pulse and Periodicity Detection

A comparison of the two techniques is best done by considering the ratio of the two signal-to-noise ratios:

$$\begin{aligned} r &\equiv \frac{(S/N)_{\text{SP}}}{(S/N)_{\text{FFT}}} \\ &= \left(\frac{2\eta}{\zeta N_p^{1/2}} \right) \frac{S_{\text{max}}}{S'_{\text{avg}}} \\ &= \left(\frac{1}{N_p} \right)^{1/2} \frac{2\eta S_{\text{max}}}{\zeta (1 - N_p^{-1})^{-1} \int_0^{S_{\text{max}}} dS S f_S(S)}. \end{aligned} \quad (\text{A9})$$

Unimodal Distributions

Inspection of Eq. A9 indicates that in order for $r > 1$, $S_{\max}/S'_{\text{avg}} > \zeta N_p^{1/2}/2\eta$, which is a large number for typical observation times T and pulse periods P . Some unimodal PDFs satisfy this criterion for large N_p while many do not.

We first consider an *exponential* PDF,

$$f_S(S) = S_{\text{avg}}^{-1} e^{-S/S_{\text{avg}}} U(S), \quad (\text{A10})$$

where U is the unit step function. For this case the maximum pulse intensity encountered in N_p trials is

$$S_{\max} = S_{\text{avg}} \ln N_p, \quad (\text{A11})$$

the renormalized average is

$$S'_{\text{avg}} = S_{\text{avg}} \left[1 - \frac{\ln N_p}{N_p - 1} \right] \quad (\text{A12})$$

and ratio of S/N for the two search methods becomes

$$r = \frac{2\eta \ln N_p}{\zeta N_p^{1/2} [1 - \ln N_p / (N_p - 1)]}. \quad (\text{A13})$$

For this case, $r > 1$ only for $N_p \leq 47$.

We next consider a *power law* PDF. A truncated power law PDF can be written in the form

$$f_S(S) = \mathcal{N} S^{-\alpha}, \quad S_1 \leq S \leq S_2 \quad (\text{A14})$$

$$\mathcal{N} = \begin{cases} (\ln S_2/S_1)^{-1} & \alpha = 1 \\ \frac{(1-\alpha)}{(S_2^{1-\alpha} - S_1^{1-\alpha})} & \alpha \neq 1. \end{cases} \quad (\text{A15})$$

For a flat PDF ($\alpha = 0$) all pulse intensities are equally probable, so we expect that as N_p gets large, the maximum and minimum intensities will equal the cutoff values. Letting $S_{\max} \rightarrow S_2$, we find

$$r = \frac{4\eta}{\zeta N_p^{1/2}} \frac{1}{(1 + S_1/S_2)}. \quad (\text{A16})$$

Asymptotically, the maximum r results for $S_2/S_1 \gg 1$,

$$r_{\max} \rightarrow \frac{4\eta}{\zeta N_p^{1/2}}, \quad (\text{A17})$$

which yields $r > 1$ only for $N_p < 11$.

We will not consider power laws with $\alpha < 0$. For $\alpha > 0$, larger amplitudes are less probable, so we expect that the maximum encountered out of N_p pulses generally will be less than S_2 . We find that

$$S_{\max} = \begin{cases} S_1 \left(\frac{S_2}{S_1} \right)^{1-N_p^{-1}}, & \alpha = 1 \\ \frac{S_2}{\left[\left(\frac{N_p - 1}{N_p} \right) \left(1 + \left(\frac{S_2}{S_1} \right)^{\alpha-1} \frac{1}{N_p - 1} \right) \right]^{\frac{1}{\alpha-1}}} & \alpha \neq 1 \end{cases} \quad (\text{A18})$$

Using S_{\max} we evaluate³ S'_{avg}

$$S'_{\text{avg}} = \begin{cases} \frac{S_{\max} - S_1}{\ln S_{\max}/S_1} & \alpha = 1 \\ \frac{S_1 S_{\max} \ln S_{\max}/S_1}{S_{\max} - S_1} & \alpha = 2 \\ S_{\max} \left(\frac{\alpha-1}{\alpha-2} \right) \left[\frac{\left(\frac{S_{\max}}{S_1} \right)^{\alpha-2} - 1}{\left(\frac{S_{\max}}{S_1} \right)^{\alpha-1} - 1} \right] & \alpha \neq 1, 2. \end{cases} \quad (\text{A19})$$

³ Note that we evaluate S'_{avg} by integrating from the actual lower cutoff S_1 to the effective upper cutoff S_{\max} . This is valid only for monotonically decreasing PDFs, i.e. $\alpha > 0$. For a flat PDF, moreover, we should let $S_{\max} \rightarrow S_2$.

For steeper power laws with $\alpha > 0$, the S/N ratio $r > 1$ only for small N_p for $\alpha \lesssim 1$. For intermediate cases, $1.5 \lesssim \alpha \lesssim 2.5$, r has a maximum at $N_p \gg 1$. For steep power laws (e.g. $\alpha \geq 3$) the ratio $r > 1$ again only for small N_p and decreases monotonically.

Figure A12 shows r for several power-law cases and for the exponential PDF and illustrates the statements made in the preceding paragraph. The values for r are small for nearly flat PDFs because the pulses Fourier-analyzed in a long-train of pulses have amplitudes that do not deviate much from the peak pulse. For very steep power laws (e.g. $\alpha \geq 3$), the probability of seeing a large pulse near the upper cutoff, S_2 , is too small to outweigh the $N_p^{1/2}$ increase in S/N of the Fourier method, even for very large N_p . For intermediate cases, where r has a distinct maximum, the likelihood of seeing a large pulse outweighs the $N_p^{1/2}$ increase in S/N of the Fourier method.

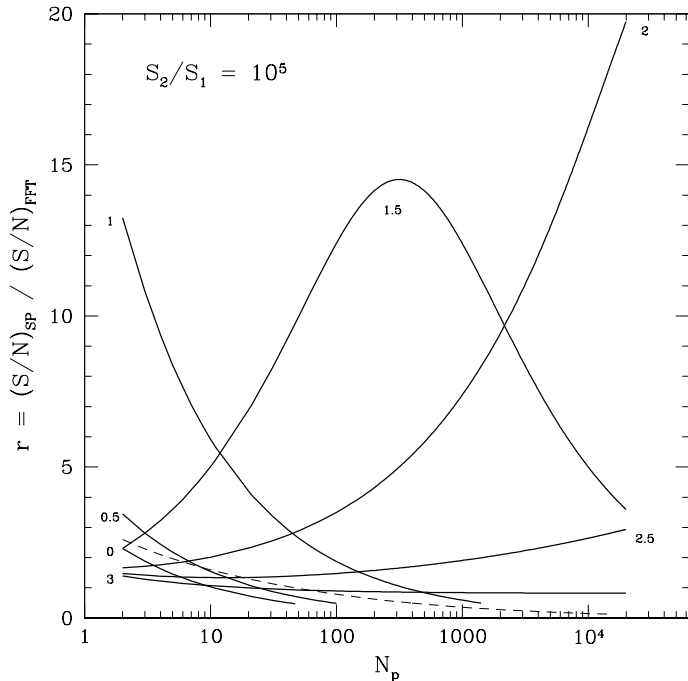


FIG. A12.— The S/N ratio r for power-law intensity PDFs (solid lines) and for an exponential PDF (dashed line). The exponent of the PDF α is shown and all power-laws are for a ratio of cutoff intensities $S_2/S_1 = 10^5$. Single-pulse detection is superior to a Fourier harmonic-sum detection scheme if $r > 1$.

For $\alpha > 1$ and $\alpha \neq 2$ we can express r in the limit where $S_2/S_1 \gg 1$ using Eq. A18-A19:

$$r \approx \left(\frac{2\eta}{\zeta}\right) \left(\frac{\alpha-2}{\alpha-1}\right) \times \begin{cases} N_p^{\frac{3-\alpha}{2(\alpha-1)}}, & N_p \ll (S_2/S_1)^{\alpha-1} \\ \left(\frac{S_2}{S_1}\right) N_p^{-1/2}, & N_p \gg (S_2/S_1)^{\alpha-1}. \end{cases} \quad (\text{A20})$$

For small N_p , r scales as $r \propto N_p^{(3-\alpha)/2(\alpha-1)}$ until $S_{\max} \rightarrow S_2$ and then r decreases as $N_p^{-1/2}$. Note that r has an increasing branch only if $1 < \alpha < 3$, consistent with Figure A12. If there is an increasing branch, then we expect a maximum approximately where the two scaling laws in Eq. A20 are equal:

$$N_{p_{\max}} \approx \left(\frac{S_2}{S_1}\right)^{\alpha-1}. \quad (\text{A21})$$

For $S_2/S_1 = 10^5$, we expect the maximum for $\alpha = 3/2$ to be at $N_p \approx 10^{5/2}$, consistent with the exact expressions evaluated in the Figure. The maxima for $\alpha = 2$ and $\alpha = 5/2$ are then expected at $N_{p_{\max}} \approx 10^5$ and $10^{15/2}$ and are thus off the scale of Figure A12.

We conclude that for certain power laws, intensity cutoffs and numbers of pulses, single-pulse searches can be superior to periodicity searches.

For the Crab pulsar at 146 MHz, Argyle & Gower (1972) find $\alpha \approx 2.5$ over at least two orders of magnitude of flux density (c.f. Figure 4-9 of Manchester & Taylor 1977). This slope is consistent with the fact that the Crab pulsar is more easily detected (and was discovered through) using its giant pulses. At 812 MHz Lundgren et al. (1995) find $\alpha \approx 3.5$ over 1.2 orders of magnitude. They also infer that the PDF for all pulses (giant and normal) is bimodal. Therefore, even though the slope found by Lundgren et al. would suggest that single-pulse detection would be inferior to a periodicity search, the apparent bimodality appears to change this conclusion, as we show below.

Bimodal Distribution

A bimodal distribution provides a finite phase space for $r > 1$, even for large pulse numbers $N_p \gg 1$. Consider the bimodal distribution

$$f_S(S) = (1 - g)\delta(S - S_1) + g\delta(S - S_2). \quad (\text{A22})$$

The only interesting case is when the interval contains at least one pulse with intensity S_2 , requiring $gN_p \gtrsim 1$ or $g > g_{\min}$ where $g_{\min} = N_p^{-1}$. In this case we have

$$r = \frac{2\eta S_2}{\zeta N_p^{1/2} [(1 - g)S_1 + gS_2]}. \quad (\text{A23})$$

To have $r > 1$ requires $g_{\min} < g < g_{\max}$ where

$$g_{\max} = \frac{(2\eta/\zeta)N_p^{-1/2} - S_1/S_2}{1 - S_1/S_2}. \quad (\text{A24})$$

Figure A13 shows regions in the two dimensional space of g and S_1/S_2 for which $r > 1$. The regions are a function of N_p .

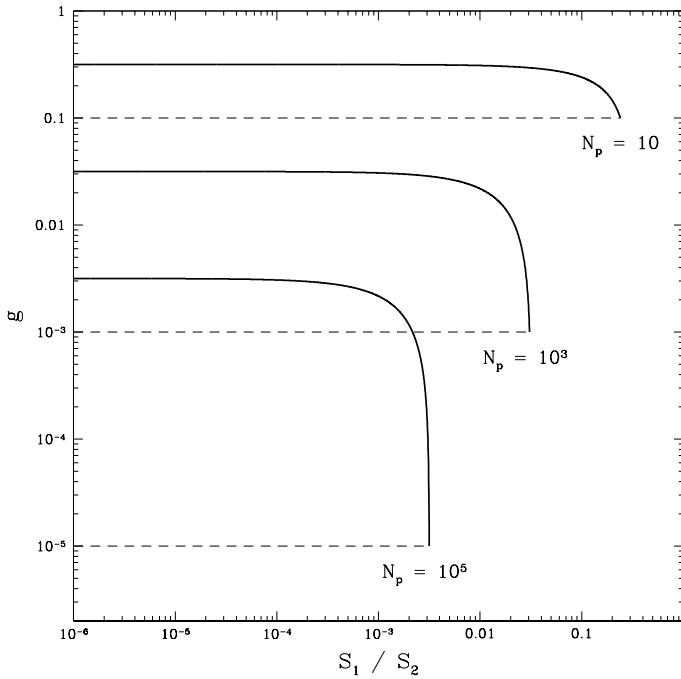


FIG. A13.— Domain for which a single-pulse search is more sensitive than a periodicity search. The pulse intensity distribution is assumed to be bimodal. S_1 is the intensity of ordinary pulses with probability $1 - g$ and S_2 is the giant-pulse intensity with probability g . The results depend on how many pulse periods, N_p , are analyzed. For each of the three cases shown, a single-pulse search is superior for values of g and S_1/S_2 between the dashed and solid lines.

A special case of interest for the bimodal PDF is where the lowest intensity pulses are null pulses (i.e. $S_1 = 0$). Then

$$r = \frac{2\eta}{g\zeta N_p^{1/2}}. \quad (\text{A25})$$

Single pulse detection is superior to a periodicity search when

$$N_p^{-1} < g < (2\eta/\zeta)N_p^{-1/2}. \quad (\text{A26})$$

This regime corresponds to values of g between the solid and dashed lines in Figure A13 for small values of S_1/S_2 .

Under some other special circumstances, searches for single pulses are more effective than periodicity searches. For large duty cycles, the single-pulse detection scheme becomes exponentially better once the pulse width exceeds the pulse period. Using the general expressions in Eq. A5 through Eq. A7 when calculating r as a function of duty cycle, W/P , we find as a typical trend that the periodicity search is superior for $W/P \lesssim 1$ and if the single-pulse amplitude PDF does not have a large dynamic range in amplitudes, as described in the previous subsection. However, for $W/P \gtrsim 1$, the single-pulse search is generally superior, no matter the form for the amplitude PDF.

These results imply that sources with small spin and small orbital periods may be detected in single-pulse searches when they would be missed completely in periodicity searches. Similarly, distant pulsars viewed through deep scattering volumes and thus having large scattering measures are likely to be missed in periodicity searches. In this case, the scattering time is a strong function of frequency, and so too will be the relative sensitivities of single-pulse and periodicity searches.

TABLE 1
RADIO PULSARS WITH HIGHEST B_{lc}

Name	P (ms)	\dot{P} (10^{-15} s s $^{-1}$)	B_{lc} (10^5 Gauss)
B1937+21	1.56	1.1×10^{-4}	9.8
B0531+21	33.4	4.2×10^2	9.3
B1821-24	3.05	1.6×10^{-3}	7.2
B1957+20	1.61	1.7×10^{-5}	3.6
B0540-69	50.4	4.8×10^2	3.5
J0218+4232	2.32	7.5×10^{-5}	3.1
J1823-3021A	5.44	3.4×10^{-3}	2.5
J0034+0534	1.88	6.7×10^{-6}	1.6
J2229+6114	51.6	7.8×10^1	1.3
J0205+6449	65.7	1.9×10^2	1.2

TABLE 2
POINTINGS AT M33

N	RA	DEC	N_p	Total time (s)
1	01:33:51	30:59:52	7	8100
2	01:33:37	30:53:07	6	7800
3	01:34:04	30:53:07	8	10800
4	01:33:24	30:46:22	8	10800
5	01:33:51	30:46:22	8	10800
6	01:34:18	30:46:22	5	6300
7	01:33:10	30:39:37	7	9000
8	01:33:37	30:39:37	6	6300
9	01:34:04	30:39:37	8	8100
10	01:34:31	30:39:37	10	9900
11	01:33:24	30:32:52	8	8100
12	01:33:51	30:32:52	6	7200
13	01:34:18	30:32:52	7	7800
14	01:33:38	30:26:07	7	8100
15	01:34:04	30:26:07	6	7200
16	01:33:51	30:19:22	7	8100
off1	00:33:00	30:59:52	2	3600
off2	02:33:51	30:59:52	3	3600

TABLE 3
POINTINGS AT OTHER GALAXIES

Name	RA	DEC	l	b	D (Mpc)	N_p
NGC253	00:47:33.1	-25:17:18	97.3	-88.0	3	3
NGC300	00:54:53.5	-37:41:00	299.2	-79.4	2	2
Fornax	02:39:34	-34:31:08	237.3	-65.7	16.9	1
LMC	05:33:14 [†]	-69:21:38 [†]	279.4	-32.17	0.050	6
NGC6300	17:16:59.2	-62:49:11	328.5	-14.1	16.9	1
NGC7793	23:57:49	-32:35:24	4.6	-77.2	3.5	3

[†]Coordinates of the central LMC pointing.